American Mineralogist, Volume 88, pages 653–666, 2003

Model pyroxenes I: Ideal pyroxene topologies

RICHARD M. THOMPSON* AND ROBERT T. DOWNS

Department of Geosciences, University of Arizona, Tucson, Arizona 85721-0077, U.S.A.

ABSTRACT

Ideal pyroxenes are hypothetical structures based on ideal closest-packed arrangements of O anions. They are modeled after observed pyroxene structures and have the general formula $M2M1T_2O_6$, where M2 and M1 represent octahedrally coordinated cations, and T represents tetrahedrally coordinated cations. An algorithm has been created to construct all possible ideal pyroxenes based on closest-packed stacking sequences of length 12 or less. These structures are reported.

The only significant structural parameters that vary between different ideal pyroxenes are the M1-T and M2-T distances. We show that the repulsive forces between these pairs of cations distinguishes the energetics of the ideal pyroxenes and may be important in determining the topologies of observed pyroxenes.

INTRODUCTION

The term pyroxene refers to a group of crystal structures that include important components of the Earth's crust and mantle, lunar and Martian rocks, and meteorites (Deer et al. 1978). Many pyroxene phases not found in nature have been synthesized. There are several naturally occurring polymorphs. These commonly display $P2_1/c$, $C2/c$, *Pbcn*, or *Pbca* symmetry. More rarely, cation ordering at a given site results in $P2/n$ symmetry. These polymorphs have been described in detail by Cameron and Papike (1981), and at elevated pressure and temperature by Yang and Prewitt (2000).

We are interested in the so-called "ideal pyroxenes" (Thompson 1970; Papike et al. 1973) and their relationships to observed structures. Ideal pyroxenes are hypothetical structures based on ideal closest-packed arrangements of O anions. They have the general formula $M2M1T_2O_6$, where M2 and M1 represent octahedrally coordinated cations, and T represents tetrahedrally coordinated cations.

We establish a working definition of "ideal pyroxene" by describing and illustrating the structural features and relationships that can be used as building blocks to derive crystal structures for these hypothetical constructs. Two of the defining structural elements in ideal pyroxenes are chains of edge-sharing octahedra and corner-sharing tetrahedra that run parallel to **c**. These chains can be constructed by placing cations in the interstitial voids between closest-packed monolayers of anions stacked along **a***. The cation sites in a given chain are related to each other by a *c*-glide perpendicular to **b**. This is the only symmetry element common to all possible ideal pyroxene structures. In many ideal pyroxenes, it is the only symmetry element.

The arrangements of anions in these ideal structures can be described as stacking sequences of closest-packed monolayers, denoted A, B, and C in the traditional way (Patterson and Kasper 1959). For example, the anion arrangement in ideal $P2_1cn$ protopyroxene can be described by the stacking sequence ABAC. Since all of the cations between a given pair of monolayers are exclusively tetrahedral or octahedral, we can modify the traditional ABC stacking sequence symbolism with superscripted Ts or Os to indicate tetrahedral or octahedral cation layers, respectively. The complete ideal $P2_1cn$ protopyroxene can be described as $A^OB^TA^OC^T$, with octahedrally coordinated cations between AB and AC and tetrahedrally coordinated cations between BA and CA.

It will be important to our discussion to distinguish between monolayer sandwiches with identical letters reversed, e.g., AB and BA. We define AB to mean that the atoms in the A-layer have smaller *x*-coordinates than those in the B-layer, and vice versa for BA. It will also be important to distinguish between the stacking sequence ABAC and the stacking sequence label ABAC. The former refers to the physical structure, a unique closest-packed arrangement of O anions; the latter refers to the four letters that represent the structure. The label can be manipulated using certain rules that represent changes of basis to derive equivalent labels representing the same stacking sequence or structure (Thompson and Downs 2001b). In this example, BABC, CBCA, ACAB, etc. all represent the same structure. Similarly, "pyroxene $A^OB^TA^OC^T$" refers to the unique physical structure, while "pyroxene label $A^OB^TA^OC^T$" refers to the non-unique sequence of letters representing that structure.

In an ideal pyroxene, we define the basal faces of the tetrahedra as the faces parallel to (100). The two anions that are shared with other tetrahedra at the corners of these basal faces are referred to as the bridging O3 anions (Fig. 1). The nonbridging basal anions are referred to as O2 and the apical anions as O1. This nomenclature is consistent with the traditional labeling of atoms in observed structures.

The chain-forming symmetrically equivalent edge-sharing octahedral sites are called M1 and are related to each other by

* E-mail: Thompson@geo.arizona.edu

0003-004X/03/0004–653$05.00

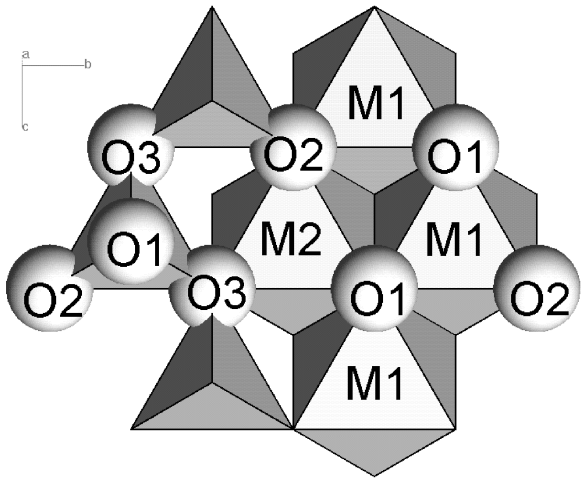

FIGURE 1. A portion of an ideal pyroxene structure viewed along **a***. The $M1O_6$ and $M2O_6$ groups are illustrated as octahedra and TO_4 groups as tetrahedra. Representative O atoms are illustrated as spheres and are labeled to indicate nomenclature.

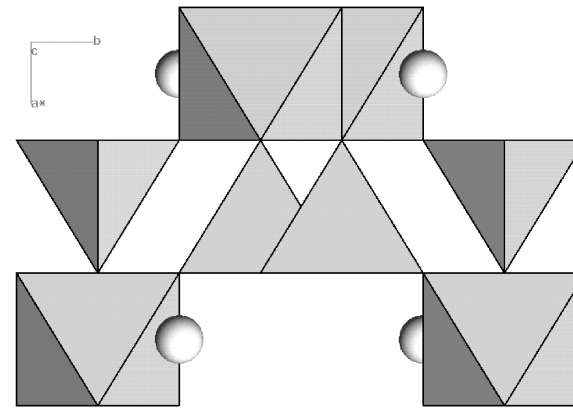

FIGURE 2. A portion of an ideal pyroxene structure viewed along **c**. Tetrahedra bridge the adjacent octahedral chains in three dimensions, connecting the pyroxene structure. The $M1O_6$ groups are illustrated as octahedra, and M2 as a sphere.

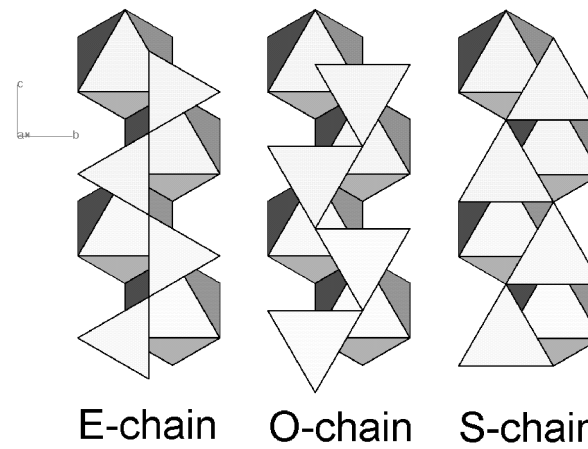

FIGURE 3. Portions of three different model pyroxene structures viewed along **a*** to illustrate chain configurations. An E-chain has an O3-O3-O3 angle of 180°, and is not closest-packed. An O-chain has an O3-O3-O3 angle of 120° and is cubic closest-packed. An S-chain has an O3-O3-O3 angle of 240° and is hexagonal closest-packed. In order to avoid confusion when determining O3-O3-O3 angles, imagine that **c** points north and **b** points east. The O3-O3-O3 angle is determined by any two adjacent tetrahedra that are pointing along –**a*** and have a southeastern and a northwestern orientation relative to each other.

the *c*-glide running up the middle of the chain. Tucked into the kinks of the M1 chains are additional cation sites referred to as M2. They are also related to each other by the *c*-glide, but do not form continuous chains. In an ideal pyroxene structure, both M1 and M2 are at the centers of perfect octahedra. However, electron density analysis of observed structures has shown that M2 can have four, five, six, or eight coordination (Downs 2003). Adjacent octahedral chains within a given monolayer sandwich are linked by basal faces of tetrahedral chains in the monolayer sandwiches above and below (Fig. 2). This connects the structure in the **b** direction. The apical anions of the tetrahedral chains are shared with octahedral chains so that the tetrahedra also connect the structure in the **a*** direction.

Thompson (1970) noted that in many observed pyroxenes, the O3-O3-O3 angle is about 180°. He called these "extended structures" and we refer to this sort of tetrahedral chain as an E-chain (Fig. 3) after Papike et al. (1973). Thompson (1970) made model pyroxene chains with regular M1 and T. He pointed out that a rotation of the tetrahedra in a model E-chain in either direction by 30° about an axis passing through the apical O1 anion perpendicular to the (100) plane brings the anions into a closest-packed arrangement. If the basal faces of the rotated tetrahedra point in the same direction as the closest parallel octahedral faces in the octahedral chain at the apices of the tetrahedral chain, then he called the rotation an S-rotation and we call the tetrahedral chain an S-chain. A 30° rotation in the opposite sense leaves the tetrahedral basal faces pointing opposite to the octahedral faces and is called an O-rotation, producing an O-chain.

It has become commonplace to use the O3-O3-O3 angles in natural pyroxenes as a way to quantify the degree of S- or O-rotation (Thompson 1970; Papike et al. 1973; for more recent examples c.f. Arlt and Angel 2000; Tribaudino et al. 2002). If a tetrahedral chain in a pyroxene is O-rotated, then its O3-O3-O3 angle is described as less than 180°, while an S-rotated chain is described as having an O3-O3-O3 angle greater than 180°. Although each tetrahedron in a fully rotated chain is only rotated 30° from the extended chain position, the resulting O3-O3-O3 angle is formed by two tetrahedra so a fully rotated O-chain has an O3-O3-O3 angle of 120°, while a fully rotated S-chain has an O3-O3-O3 angle of 240°. Papike et al. (1973) pointed out that a fully rotated structure containing only S-chains is hexagonal closest-packed and a fully rotated structure containing only O-chains is cubic closest-packed.

Thompson (1970) used, but did not define, the term "tilt" to

describe the orientation of the octahedra in pyroxenes. Papike et al. (1973) compared Thompson's (1970) ideal pyroxenes to real pyroxenes and formalized the definition of octahedral "tilt" as follows: if the lower triangular face parallel to (100) of an octahedron points in the **–c** direction, then it has a negative tilt, denoted "–tilt," and if it points in the **+c** direction, then it has a positive tilt, denoted "+tilt."

The tetrahedral chains between a given monolayer sandwich have two orientations (Fig. 2). The tetrahedra in half of the chains point down **a***, the rest point up **a***. Thompson (1970) introduced the parity rule, which states that if the chains pointing up and the chains pointing down between a given monolayer sandwich in an ideal pyroxene are rotated in the same direction (i.e., both are either S- or O-chains), then the octahedral chains above and below them must have the same tilt and if the tetrahedral chains are rotated in the opposite directions (i.e., one S- and one O-chain), then the octahedra must have opposite tilts. Thompson's parity rule only applies to ideal pyroxenes, and is not obeyed by observed pyroxenes with space groups *Pbca* and *Pbcn* (Papike et al. 1973).

Pannhorst (1979, 1981) made model pyroxene structures containing both O and E-chains. He argued that both symmetry and M2-O bonding topologies should be included in pyroxene classification schemes.

Law and Whittaker (1980) derived space groups for all possible ideal pyroxenes based on stacking sequences of length four and eight. They pointed out that octahedral tilt is arbitrarily dependent on the direction of the **c**-axis. Consider the six possible pairings of the three different closest-packed O atom monolayers: AB, BA, AC, CA, BC, and CB. If a basis is chosen so that an octahedral layer between an AB pair has a +tilt, then octahedral layers between BC and CA pairs will also have +tilts, while octahedral layers between BA, CB, and AC pairs will have –tilts. Also, if three consecutive monolayers can be described with only two different letters (i.e., ABA), then the tetrahedral chain is an S-chain, while three different letters indicates an O-chain. For example, the ideal pyroxene portion $A^{Oa}B^{T}A^{Ob}C$ has one tetrahedral layer. Half of the tetrahedra in this layer are associated with the Oa octahedral chain, half with the Ob octahedral chain. Those associated with Oa form an S-chain while those associated with Ob form an O-chain. If Oa has +tilt, then Ob has –tilt. This partial pyroxene could be described symbolically in the Law and Whittaker (1980) notation as +SO– (equivalents –SO+, –OS+, +OS– can be obtained by changing basis). Completing this pyroxene by placing a tetrahedral layer between the CA monolayer sandwich results in a pyroxene with traditional representation +SO–SO. Law and Whittaker (1980) thus established a correspondence between SO+– pyroxene representation and closest-packing representation.

The only reported crystal structure data for an ideal pyroxene prior to this study is from Hattori et al. (2000). They determined that the ideal representation of $FeGeO_3$ was cubic closest-packed (CCP) and showed that $FeGeO_3$ approached the ideal arrangement with increasing pressure. They derived the ideal structure in order to quantify the distortion of their observed crystal from ideal cubic closest-packed. No studies have presented structural data for other ideal pyroxenes.

Thompson and Downs (2001a) created an algorithm to quantify the distortion from hexagonal and cubic closest-packing in crystals provided the crystals are not too distorted. In particular, they showed that *C*2/*c* pyroxenes with eight-coordinated M2 sites rapidly move toward CCP with pressure and away from it with temperature. Under the assumption that anion-anion interactions are the principle component of the forces governing compression mechanisms in pyroxenes, we undertook a study of the ideal structures. We intended to determine if all pyroxenes move toward ideal closest-packed with pressure. Furthermore, comparing the energetics of ideal analogs may indicate why we see only a few of the many possible pyroxenes in nature and why they behave the way they do with temperature, pressure, and composition. In particular, we are searching for an understanding of the sequences of structures adopted during pyroxene-pyroxene transitions. As a first step, Thompson and Downs (2001b) created an algorithm that generates all symmetrically nonequivalent closest-packed stacking sequences of given length *N* using group theory. We have taken all of the closest-packed stacking sequences of length 12 or less and designed an algorithm to create each of the 81 possible pyroxenes based on those sequences. Our study is restricted to stacking sequences of length 12 or less because no observed pyroxenes have been reported with closest-packed analogs having longer stacking sequences.

Algorithm

Before going into detail, we present a single paragraph outline of our method. The first step is to generate all possible closest-packed stacking sequences of O anions. We then take each sequence and, working within a symmetryless orthorhombic cell, place cations in such a way as to create a valid pyroxene. We then identify all of the symmetry elements in the structure and thus determine the space group. Using a symmetry diagram of our structure and the *International Tables* (Henry and Lonsdale 1965), we create a cell and asymmetric unit in an appropriate setting.

There are some fundamental rules that govern the way ideal pyroxenes can be put together. The closest-packed monolayers of O atoms are stacked along **a***. Also along **a***, pyroxenes consist of alternating layers of tetrahedra and octahedra. Thus, all closest-packed pyroxenes must have an even number of monolayers in the repeat unit along **a***. In fact, the number of monolayers must be a multiple of four, as it is clear from Figure 2 that nearest neighbor octahedral layers are not translationally equivalent. Therefore we need only consider sequences of length 4, 8, and 12.

In some cases, a given stacking sequence produces two different pyroxenes. When building an ideal pyroxene, we start with two monolayers and place cations in chains between them. These can be either tetrahedral or octahedral chains, raising the possibility of two distinct pyroxenes. For example, pyroxene $A^{T}B^{O}A^{T}B^{O}C^{T}A^{O}B^{T}C^{O}$ has space group $P2/c$, and is topologically distinct from pyroxene $A^{O}B^{T}A^{O}B^{T}C^{O}A^{T}B^{O}C^{T}$, which has space group $P2_1/c$, yet both have the same closest-packed stacking sequence.

When we refer to a sequence in terms of As, Bs, and Cs, the particular combination of letters we use is actually just one of

many stacking sequence labels that describe the same structure. For example, label ABAC describes the same structure as BABC (or CACB, CBCA, etc.). Using group theory, Thompson and Downs (2001b) derived a set of rules that describe the relationships between equivalent stacking sequence labels. All equivalent labels for a given structure can be generated from just one label using our rules.

If a pyroxene label can be manipulated using these rules so that we arrive at the original stacking sequence label with Ts and Os switched, then there is only one distinct pyroxene based on that stacking sequence. The caveat is that at each step in the manipulation, we must be careful to preserve the relationship between cation and anion layers. For instance, we can rewrite the pyroxene label $A^TB^OA^TB^OA^TC^OA^TC^O$ first as $C^OA^TC^OA^TB^OA^TB^OA^T$ (translating the origin five monolayers along the stacking direction), then writing this backward we get $A^OB^TA^OB^TA^OC^TA^OC^T$ (reversing the stacking direction and translating the origin one monolayer along the new stacking direction), demonstrating that the two possible pyroxenes are the same structure.

Whenever a stacking sequence label has an equivalent label that is a palindrome after appending the first letter in the next repeat unit, there is only one possible pyroxene based on the stacking sequence. A palindrome is a sequence of letters that has the same spelling forward and backward. For example, the stacking sequence label we just examined, ABABACAC, has equivalent label ABACACAB (translating the origin two monolayers along the stacking direction). When written as a pyroxene label, $A^TB^OA^TC^OA^TC^OA^TB^OA$, we see that reversing the order results in the same stacking sequence label with Ts and Os switched. Therefore, there is only one possible pyroxene.

We now consider a stacking sequence of length 12 or less with a label that does not have an equivalent palindrome. In order for this sequence to uniquely define one pyroxene, it is a necessary but not sufficient condition that the sequence label contains equal numbers of at least two different letters. As an example, ABABACABACAC contains six As, three Bs, and three Cs. Pyroxene label $A^TB^OA^TB^OA^TC^OA^TB^OA^TC^OA^TC^O$ is equivalent to $A^OC^TA^OC^TA^OB^TA^OC^TA^OB^TA^OB^T$ (reversing the stacking direction and translating the origin one monolayer along the new stacking direction). We can obtain another equivalent by renaming all Bs as Cs and vice versa giving $A^OB^TA^OB^TA^OC^TA^OB^TA^OC^TA^OC^T$ (rotating the basis 60° around the stacking vector). These operations do not affect the relationship between the anion and cation layers so this is the same structure. If the stacking sequence label has no equivalent palindrome and unequal numbers of all letters then the stacking sequence is the anion skeleton for two different pyroxenes. For stacking sequences longer than 12, we would need to consider the case where the stacking sequence label is built from four identical sublabels of odd length. Moving the origin halfway along **c** results in the same sequence with Ts and Os switched so these define only one pyroxene and need not obey the above rules (e.g., 4 × ABABABCAC).

We build our ideal pyroxenes in orthorhombic cells without using symmetry. Hereafter, we refer to these cells as "explicit cells." The number of monolayers in the stacking sequence, 4, 8, or 12, determines the length of **a** (a = number of monolayers × height of monolayer = $N \times 2\sqrt{6}r/3$, where r is the ideal anion radius). When the pyroxene is described with the appropriate space group and setting, this length remains the length of the repeat unit along **a***, i.e., the d-spacing of (100). The length of **b** is the distance across one tetrahedral chain and one octahedral chain or $6r$, and c is the length of two tetrahedra along the tetrahedral chain (i.e., twice the height of a tetrahedral basal face) or $2\sqrt{3}r$ (Fig. 4). We make the arbitrary choice that an A-layer has anions at {[x 0 0], [x 1/3 0], [x 2/3 0], [x 1/6 1/2], [x 1/2 1/2], [x 5/6 1/2]} (Fig. 4), a B-layer has anions at {[x 0 1/3], [x 1/3 1/3], [x 2/3 1/3], [x 1/6 5/6], [x 1/2 5/6], [x 5/6 5/6]}, and a C-layer has anions at {[x 1/6 1/6], [x 1/2 1/6], [x 5/6 1/6], [x 0 2/3], [x 1/3 2/3], [x 2/3 2/3]}. This choice gives octahedra between AB, BC, and CA monolayer sandwiches a +tilt, and octahedra between BA, CB, and AC sandwiches a –tilt.

When looking at the set of the symmetrically equivalent labels for a given stacking sequence, we choose to work with the one that is first when the equivalent labels are put in alphabetical order. Thus, all of our stacking sequences labels begin with AB— (Thompson and Downs 2001b).

Table 1 defines the relationships between the positions of the cations in a given layer and the positions of the cations in adjacent layers. The placement of the first tetrahedral chains in the AB layer is arbitrary. Once this is done all the other positions are fixed. We take each stacking sequence and place cations between the monolayers according to the rules of Table 1 resulting in explicit cells for all possible valid pyroxenes with stacking sequence of length 12 or less. The positions in Table 1 result from the geometric relationships between the sites in closest-packed stacking sequences but were generated empirically.

Using the software IDGROUP (Boisen et al. 1994), we determine the symmetry elements in each explicit cell. Then we construct a symmetry diagram and compare it to the *International Tables* (Henry and Lonsdale 1965) in order to identify the space group. We also use this diagram to pick our standard cell so that its setting matches the conventional choice of setting for the natural analogs to the ideal pyroxene if they exist.

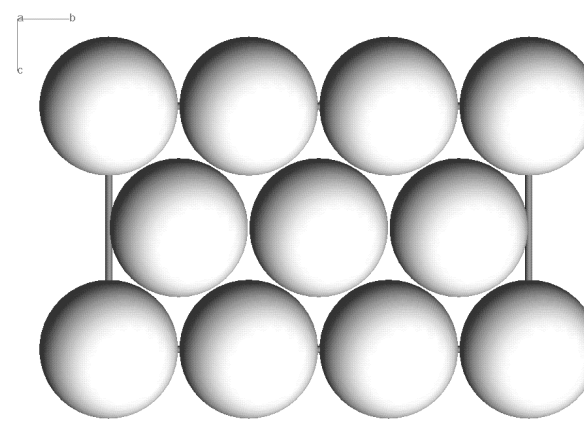

FIGURE 4. A monolayer from an ideal pyroxene viewed along **a*** showing the unit cell in the **bc** plane.

TABLE 1. The relationships between the positions of the cations in a given layer and the positions of those in adjacent layers

Monolayer sandwich	AB	AC	BA	BC	CA	CB
T_1	X1 5/6 5/6 X1 2/3 1/3 X2 1/6 1/2 X2 1/3 0	X1 2/3 2/3 X1 5/6 1/6 same as AB	X1 5/6 1/2 X1 2/3 0 X2 1/3 1/3 X2 1/6 5/6	same as AC same as BA	same as BA X2 1/3 2/3 X2 1/6 1/6	same as AB same as CA
M_1	X 2/3 2/3 X 5/6 1/6 X 1/2 1/6 X 0 2/3	X 5/6 5/6 X 2/3 1/3 X 1/2 5/6 X 0 1/3	same as AB	X 5/6 1/2 X 2/3 0 X 0 0 X 1/2 1/2	same as AC	same as BC
T_2	same as BA_{T1} with X1 and X2 switched	same as CA_{T1} with X1 and X2 switched	same as AB_{T1} with X1 and X2 switched	same as CB_{T1} with X1 and X2 switched	same as AC_{T1} with X1 and X2 switched	same as BC_{T1} with X1 and X2 switched
M_2	X 1/3 2/3 X 1/6 1/6 same as M_1	X 1/3 1/3 X 1/6 5/6 same as M_1	same as AB	X 1/6 1/2 X 1/3 0 same as M_1	same as AC	same as BC

Notes: For a given combination of two monolayers, there are two possible tetrahedral layers and two possible octahedral layers. The choice is determined by the positions of the cations in the layer above (i.e. smaller x-coordinate): $T_1 \rightarrow M_1 \rightarrow T_2 \rightarrow M_2 \rightarrow T_1$. Some of the geometric relationships between interstitial sites in closest-packed stacking sequences are reflected in the table. For instance, the octahedral sites between AB and between BA are the in the same place, although the tilt of the octahedra are different. Also, tetrahedra have the same y and z coordinates as their apical oxygen atoms, regardless of which type of monolayer contains their base. Anion layers: A = {[x 0 0], [x 1/3 0], [x 2/3 0], [x 1/6 1/2], [x 1/2 1/2], [x 5/6 1/2]}, B = {[x 0 1/3], [x 1/3 1/3], [x 2/3 1/3], [x 1/6 5/6], [x 1/2 5/6], [x 5/6 5/6]}, and C = {[x 1/6 1/6], [x 1/2 1/6], [x 5/6 1/6], [x 0 2/3], [x 1/3 2/3], [x 2/3 2/3]}. For 12-layer pyroxenes, X1 = x_O + 1/48, X2 = x_O + 3/48, and X = x_O + 1/24, where x_O = the x-coordinate of the closest monolayer with smaller x-coordinate.

If there are no natural analogs, then we use the standard setting for the space group as defined in the *International Tables* (Henry and Lonsdale 1965). This is discussed in depth below. In addition, we choose our asymmetric unit to match the observed analogs.

RESULTS

There are 81 ideal pyroxenes based on stacking sequences of length 12 or less. Structural parameters for these ideal pyroxenes are given in Tables 2–6[1], and all are in the crystal structure database. In order to present our data in reasonably compact form, we have placed the pyroxenes in Tables according to the size of their asymmetric unit. Each pyroxene is given a number for easy reference. If two different ideal pyroxenes are based on the same stacking sequence, they have the same number followed by a or b.

Table 2 contains the structural parameters for the five pyroxenes that repeat after four monolayers along **a**. However, three of these were constructed from explicit cells with 12 monolayers. One of these is ideal pyroxene no. 4, which has space group $C2/c$, is cubic closest-packed (CCP), and has stacking sequence ABCABCABCABC. It cannot be considered to be based on stacking sequence ABC as the cations do not repeat until after 12 monolayers along **a*** (Thompson and Downs 2001b). Two of the observed pyroxene topologies are natural equivalents to ideal pyroxene no. 4. These are the so-called "high-*P* clinopyroxenes" or H*P*-*C*2/*c* pyroxene, as we will refer to it (Yang and Prewitt 2000), which have six-coordinated M2 (Peacor 1968; Angel et al. 1992; Hugh-Jones et al. 1994; Downs 2003), and those that have eight-coordinated M2 such as diopside (Levien and Prewitt 1981) and hedenbergite (Zhang et al. 1997). The pyroxenes with eight-coordinated M2 cations have O3-O3-O3 angles ~165° and are closer to fully extended than fully rotated, while those that have six-coordinated M2 such as H*P*-*C*2/*c* ferrosilite (Hugh-Jones et al. 1994) have O3-O3-O3 angles ~140° or less and are closer to fully rotated than fully extended. We have shown that the eight-coordinated M2 clinopyroxenes move toward CCP with pressure and away from CCP with temperature (Thompson and Downs 2001a). CCP is unique among stacking sequences in that it has four equivalent monolayer stacking directions. In the ideal pyroxene structure, these are [1 0 $\bar{5}$] [3 0 1] [3 8 9] [3 $\bar{8}$ 9] in direct space, and (1 0 $\bar{1}$) (1 0 0) (1 3 1) (1 $\bar{3}$ 1) in reciprocal space. Origlieri et al. (2003) correlate these directions with observed directions of maximum and minimum compressibility in some pyroxenes.

The so-called "low clinopyroxenes" have space group $P2_1/c$ and are based on the stacking sequence ABABCACABCBC, displayed by the ideal equivalent pyroxene no. 3b. The structural parameters for no. 3b are in the conventional setting for easy comparison with observed crystals. As an example, the structure of spodumene exhibits $P2_1/c$ symmetry at 8.835 GPa (Arlt and Angel 2000), as illustrated in Figure 5, in which the distorted monolayers are labeled with the appropriate letters. In Figure 6, the layers labeled with each letter have been isolated and are viewed by themselves along the stacking vector, illustrating that they are distorted equivalents of each other.

"High clinopyroxene" or "H*T*-*C*2/*c* pyroxene," as we will refer to it (Yang and Prewitt 2000), has space group $C2/c$ and a

[1]For a copy of Tables 5 and 6, document item AM-03-027, contact the Business Office of the Mineralogical Society of America (see inside front cover of recent issue) for price information. Deposit items may also be available on the American Mineralogist web site at http://www.minsocam.org.

TABLE 2. Structural parameters of ideal pyroxenes that repeat after four monolayers down **a**

Pyroxene no.		1	2	3a	3b	4
Space group		*C*2/*c*	*$P2_1cn$	*P*2/*c*	*$P2_1/c$*	*C*2/*c*
Stacking sequence		ABAB	ABAC	ABABCACABCBCTO	ABABCACABCBCOT	ABCABCABCABC
a		$\sqrt{164/3}r$	$8\sqrt{6}r/3$	$2\sqrt{11}r$	$4\sqrt{3}r$	$2\sqrt{11}r$
cosβ		$-d/a$	0	$-d/(3a)$	$-2d/(3a)$	$-d/(3a)$
β		117.94	90	100.025	109.47	100.025
TA	*x*	5/16	11/16	11/16	1/16	5/16
	y	1/12	11/12	7/12	1/3	1/12
	z	19/48	5/6	5/16	3/8	3/16
TB	*x*		5/16	13/16	9/16	
	y		1/12	11/12	5/6	
	z		0	1/48	5/24	
M1A	*x*	0	0	0	1/4	0
	y	11/12	1/12	7/12	2/3	11/12
	z	1/4	2/3	3/4	1/6	1/4
M2A	*x*	0	0	0	1/4	0
	y	1/4	1/4	1/4	0	1/4
	z	1/4	1/6	3/4	1/6	1/4
M1B	*x*			1/2		
	y			1/12		
	z			3/4		
M2B	*x*			1/2		
	y			3/4		
	z			3/4		
O1A	*x*	1/8	7/8	7/8	7/8	1/8
	y	1/12	11/12	7/12	1/3	1/12
	z	5/24	5/6	3/8	1/4	1/8
O2A	*x*	3/8	5/8	5/8	1/8	3/8
	y	1/4	3/4	3/4	1/2	1/4
	z	7/24	0	11/24	1/4	3/8
O3A	*x*	3/8	5/8	5/8	1/8	3/8
	y	11/12	11/12	5/12	1/3	1/12
	z	7/24	1/2	11/24	3/4	7/8
O1B	*x*		1/8	5/8	3/8	
	y		1/12	1/12	5/6	
	z		0	11/24	1/12	
O2B	*x*		3/8	7/8	5/8	
	y		1/4	1/4	0	
	z		1/6	3/8	5/12	
O3B	*x*		3/8	7/8	5/8	
	y		11/12	11/12	2/3	
	z		1/6	3/8	5/12	

Note: All have four monolayers in the given unit cells. Pyroxenes 1 and 2 also have four monolayers in their symmetryless orthorhombic unit cells, but 3a, 3b, and 4 have 12 monolayers in their symmetryless orthorhombic unit cells. If *r* is the ideal anion radius, then b = 6*r*, c = 2 $\sqrt{3}$ *r*, $\alpha = \gamma = 90$. Pyroxenes 3a and 3b are constructed from the same stacking sequence: 3a is built with tetrahedral chains between the first AB monolayer sandwich and 3b with octahedral chains. Pyroxene 1 is hexagonal closest-packed and 4 is cubic closest-packed.

* Space group *$P2_1cn$* has an origin shift of [0 1/4 0] from the standard setting in the *International Tables for X-ray Crystallography* (1965).

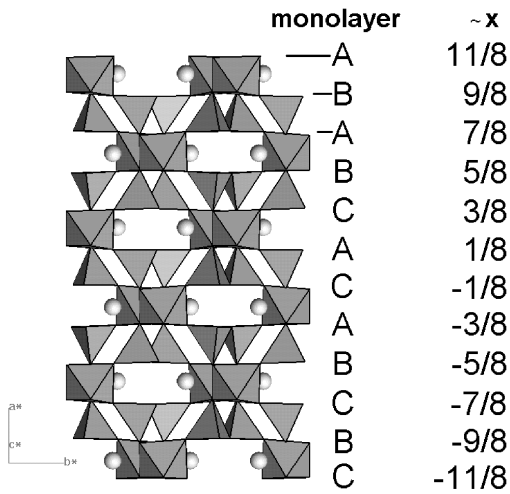

FIGURE 5. A portion of the *$P2_1/c$* spodumene structure viewed along **c** at 8.835 GPa (Arlt and Angel 2000), illustrating the stacking sequence ABABCACABCBC.

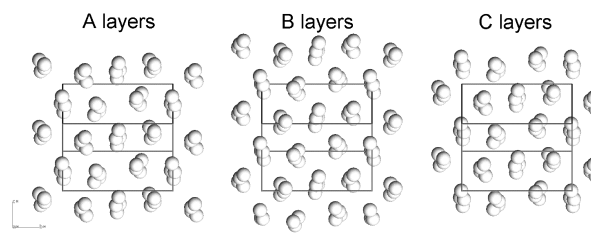

FIGURE 6. An illustration of the three types of anion monolayers from the *$P2_1/c$* spodumene structure viewed along **a*** at 8.835 GPa (Arlt and Angel 2000). The portion of the figure labeled "A layers" represents the anions from the monolayers labeled "A" in Figure 5, and similarly for the portions labeled "B layers" and "C layers." The figure demonstrates the distortion from ideal ABABCACABCBC closest-packing.

TABLE 3. Structural parameters of ideal pyroxenes that have space group *Pc* and repeat after eight monolayers down **a**

Pyroxene	5			6		
Stacking sequence	ABABABAC			ABABACBC		
	x	*y*	*z*	*x*	*y*	*z*
TA	31/32	11/12	1/6	31/32	11/12	1/6
TB	29/32	5/12	0	29/32	5/12	0
M1A	13/16	1/12	1/3	13/16	1/12	0
M2A	13/16	3/4	1/3	13/16	3/4	0
TC	23/32	7/12	5/6	23/32	5/12	2/3
TD	21/32	11/12	1/2	21/32	1/12	1/3
M1B	9/16	7/12	1/6	9/16	5/12	1/3
M2B	9/16	1/4	1/6	9/16	3/4	1/3
TE	13/32	7/12	1/2	13/32	7/12	1/2
TF	15/32	1/2	1/3	15/32	1/2	1/3
M1C	5/16	1/12	2/3	5/16	1/12	2/3
M2C	5/16	3/4	2/3	5/16	3/4	2/3
TG	5/32	1/12	0	5/32	1/12	0
TH	7/32	5/12	1/3	7/32	5/12	1/3
M1D	1/16	5/12	2/3	1/16	5/12	2/3
M2D	1/16	1/4	1/6	1/16	1/4	1/6
O1A	7/8	11/12	1/6	7/8	11/12	1/6
O2A	0	3/4	0	0	3/4	0
O3A	0	1/12	0	0	1/12	0
O1B	0	5/12	0	0	5/12	0
O2B	7/8	7/12	1/6	7/8	7/12	1/6
O3B	7/8	3/4	2/3	7/8	3/4	2/3
O1C	5/8	5/12	1/3	5/8	5/12	2/3
O2C	3/4	3/4	0	3/4	1/4	5/6
O3C	3/4	5/12	0	3/4	5/12	1/3
O1D	3/4	1/12	0	3/4	1/12	1/3
O2D	5/8	3/4	1/3	5/8	1/4	1/6
O3D	5/8	1/12	1/3	5/8	11/12	1/6
O1E	1/2	5/12	0	1/2	5/12	0
O2E	3/8	3/4	1/3	3/8	3/4	1/3
O3E	3/8	5/12	1/3	3/8	5/12	1/3
O1F	3/8	1/12	1/3	3/8	1/12	1/3
O2F	1/2	3/4	0	1/2	3/4	0
O3F	1/2	1/12	0	1/2	1/12	0
O1G	1/4	1/12	0	1/4	1/12	0
O2G	1/8	3/4	1/3	1/8	3/4	1/3
O3G	1/8	1/12	1/3	1/8	1/12	1/3
O1H	1/8	5/12	1/3	1/8	5/12	1/3
O2H	1/4	1/4	1/2	1/4	1/4	1/2
O3H	1/4	5/12	0	1/4	5/12	0

Note: If *r* is the ideal anion radius, then $a = 16\sqrt{6}\,r/3$, $b = 6r$, $c = 2\sqrt{3}r$, $\alpha = \beta = \gamma = 90$.

bonding topology (Downs, submitted) like that of ideal pyroxene no. 1, is based on stacking sequence ABAB. Nearly fully extended tetrahedral chains characterize these structures. The terms "high" and "low" come from temperature relationships between the structures (cf. Smyth 1974). Examples of H*T*-*C*2/*c* pyroxene are jadeite at room temperature (Clark et al. 1969) and H*T*-*C*2/*c* clinoferrosilite at 1050 °C (Sueno et al. 1984). Although these observed pyroxenes have bonding topologies like ideal pyroxene no. 1, the H*T*-*C*2/*c* pyroxenes with sodium at the M2 site have an O atom arrangement closer to CCP than HCP at ambient conditions.

The only orthorhombic symmetries exhibited by the ideal pyroxenes in our study are $P2_1cn$ and $P2_1ca$. Protopyroxene and orthopyroxene cannot truly be described as distorted ideal closest-packed structures because their topologies violate the parity rule, resulting in symmetries *Pbcn* and *Pbca*, respectively, and these symmetries are not found in any ideal pyroxene. We therefore call them "related structures" to the ideal pyroxenes that are the closest topological matches. They can be modeled with combinations of fully extended chains and O-chains as suggested by Pannhorst (1979). Thompson (1970) predicted that protopyroxene (space group *Pbcn*) would transform to a structure with space group $P2_1cn$ under pressure. This transformation was observed by Yang et al. (1999) for $Mg_{1.54}Li_{0.23}Sc_{0.23}Si_2O_6$ between 2.03 and 2.5 GPa. The $P2_1cn$ pyroxene is based on stacking sequence ABAC (ideal pyroxene no. 2) and protopyroxene is a related structure.

Tables 3 and 4 contain all of the ideal pyroxenes that repeat after eight monolayers along **a** and **a***. Ideal pyroxene no. 10 is Thompson's (1970) predicted inversion form for orthopyroxene. It has space group $P2_1ca$ and stacking sequence ABACBABC. Orthopyroxene is a related structure. Table 5 contains all of the ideal pyroxenes that repeat after twelve monolayers along **a** and **a*** and do not adopt *Pc* symmetry. Those that have space

TABLE 4. Structural parameters of ideal pyroxenes that have space groups other than *Pc* and repeat after eight monolayers down **a**.

Pyroxene	7			8a			8b			9a			9b			10		
Space group	$P2_1ca$			$P2/c$			$P2_1/c$			$P2/c$			$P2_1/c$			*$P2_1ca$		
Stacking sequence	ABABACAC			ABABCABC - TO			ABABCABC - OT			ABABCBAC - TO			ABABCBAC - OT			ABACBABC		
	x	y	z	x	y	z	x	y	z	x	y	z	x	y	z	x	y	z
*7*A	31/32	11/12	11/12	29/32	11/12	1/12	31/32	1/6	1/3	29/32	11/12	1/12	31/32	1/6	1/3	9/32	1/6	7/12
*7*B	29/32	5/12	3/4	27/32	5/12	11/12	15/32	1/3	1/6	27/32	5/12	11/12	15/32	1/6	1/3	7/32	2/3	5/12
*M1*A	5/16	1/12	5/12	0	5/12	1/4	7/8	2/3	1/2	0	5/12	1/4	7/8	2/3	1/2	1/8	1/3	5/12
*M2*A	5/16	3/4	5/12	0	1/4	3/4	7/8	0	1/2	0	1/4	3/4	7/8	0	1/2	1/8	0	5/12
*7*C	5/32	1/12	3/4	13/32	11/12	3/4	9/32	1/3	1/6	13/32	11/12	3/4	9/32	1/3	1/6	15/32	1/6	1/4
*7*D	7/32	5/12	1/12	11/32	7/12	1/12	7/32	2/3	1/2	11/32	7/12	5/12	7/32	2/3	1/2	17/32	5/6	7/12
*M1*B	1/16	5/12	5/12	1/4	11/12	1/12	3/8	2/3	1/6	1/4	11/12	1/12	3/8	2/3	5/6	7/8	2/3	3/4
*M2*B	1/16	1/4	11/12	1/4	1/4	1/12	3/8	0	1/6	1/4	1/4	1/12	3/8	0	5/6	7/8	1/2	1/4
*M1*C				1/2	7/12	3/4				1/2	7/12	3/4						
*M2*C				1/2	1/4	3/4				1/2	1/4	3/4						
O1A	7/8	11/12	11/12	13/16	11/12	1/12	1/16	1/6	1/3	13/16	11/12	1/12	1/16	1/6	1/3	3/16	1/6	7/12
O2A	0	3/4	3/4	15/16	3/4	11/12	15/16	0	1/6	15/16	3/4	11/12	15/16	0	1/6	5/16	0	5/12
O3A	0	1/12	3/4	15/16	1/12	11/12	15/16	1/3	1/6	15/16	1/12	11/12	15/16	1/3	1/6	5/16	1/3	5/12
O1B	0	5/12	3/4	15/16	5/12	11/12	3/16	1/3	1/6	15/16	5/12	11/12	3/16	1/3	1/6	5/16	2/3	5/12
O2B	7/8	7/12	11/12	13/16	1/4	1/12	5/16	1/2	0	13/16	1/4	1/12	5/16	1/2	0	3/16	1/2	7/12
O3B	7/8	3/4	5/12	13/16	7/12	1/12	5/16	1/3	1/2	13/16	7/12	1/12	5/16	1/3	1/2	3/16	5/6	7/12
O1C	1/4	1/12	3/4	5/16	11/12	3/4	5/16	2/3	1/2	5/16	11/12	3/4	5/16	2/3	1/2	9/16	1/6	1/4
O2C	1/8	3/4	1/12	7/16	3/4	7/12	3/16	1/2	2/3	7/16	3/4	11/12	3/16	1/2	2/3	7/16	0	1/12
O3C	1/8	1/12	1/12	7/16	11/12	1/12	3/16	2/3	1/6	7/16	1/12	11/12	3/16	2/3	1/6	7/16	1/6	7/12
O1D	1/8	5/12	1/12	7/16	7/12	1/12	9/16	1/3	1/6	7/16	7/12	5/12	9/16	1/6	1/3	7/16	5/6	7/12
O2D	1/4	1/4	1/4	5/16	3/4	1/4	7/16	1/2	1/3	5/16	3/4	1/4	7/16	0	1/6	9/16	0	3/4
O3D	1/4	5/12	3/4	5/16	7/12	3/4	7/16	1/6	1/3	5/16	7/12	3/4	7/16	1/3	1/6	9/16	5/6	1/4

Notes: If r is the ideal anion radius, then $a = 16\sqrt{6}\,r/3$, $b = 6r$, $c = 2\sqrt{3}r$, $\alpha = \beta = \gamma = 90$.

* This setting has an origin shift of [0 ¼ 0] from standard setting for space group $P2_1ca$ in the *International Tables for X-ray Crystallography* (Henry and Lonsdale 1965).

group *Pc* are in Table 6. Tables 7 and 8 are lists designed to make it easier to look up pyroxene numbers, stacking sequences, and space groups without having to go to the structure tables. Table 7 also contains information about observed equivalent and related structures.

Pyroxene crystals occur that do not have translational periodicity along **a*** due to interleaving of regions of clinopyroxene and orthopyroxene (c.f. Iijima and Buseck 1975). These crystals may still preserve a *c*-glide so that the entire crystal could be considered one unit cell with *Pc* symmetry. Some of these crystals have regions of periodicity with repeat unit length of 27 Å in the stacking direction. This is the length of one unit cell of orthopyroxene plus one unit cell of clinopyroxene. There is no equivalent ideal pyroxene with a stacking sequence of length 12. However, the ideal pyroxene **A^{T}B^{O}ACBABC**ACAB **CACBACAB**CBCA**BCBACBCA**BABC has a related topology. It has 12 monolayers in its unit cell and 36 in the repeat unit along **a***. The repeat unit along **a*** consists of three repeat units of ideal low clinopyroxene interwoven with three repeat units of ideal pyroxene related to orthopyroxene (bold in the label). Much better models for the observed crystals can probably be derived by including E-chains.

The symmetries of ideal pyroxenes are related to the symmetries of the closest-packed anion stacking sequences they are based on. Adding cations to the sequences reduces their symmetry so the pyroxene space groups are all subgroups of the stacking sequence space groups (see Appendix for details). For a discussion of the space groups of closest-packed stacking sequences, see Patterson and Kasper (1959).

TABLE 8. Second index table of pyroxenes

No.	Sequence	SG	No.	Sequence	SG
11a	ABABABABCABC	*P2/c*	33b	ABABABCABCBC	*Pc*
11b	ABABABABCABC	$P2_1/c$	34a	ABABABCACBAC	*Pc*
12a	ABABABABCBAC	*P2/c*	34b	ABABABCACBAC	*Pc*
12b	ABABABABCBAC	$P2_1/c$	35a	ABABABCBACAC	*Pc*
13	ABABABACACAC	$P2_1cn$	35b	ABABABCBACAC	*Pc*
14a	ABABABCABABC	$P2_1/c$	36	ABABACABACAC	*Pc*
14b	ABABABCABABC	*P2/c*	37a	ABABACABACBC	*Pc*
15a	ABABABCBABAC	$P2_1/c$	37b	ABABACABACBC	*Pc*
15b	ABABABCBABAC	*P2/c*	38a	ABABACABCABC	*Pc*
16	ABABACABABAC	*Cc*	38b	ABABACABCABC	*Pc*
17a	ABABACACBCBC	*P2/c*	39	ABABACABCBAC	*Pc*
17b	ABABACACBCBC	$P2_1/c$	40a	ABABACACBABC	*Pc*
18	ABABACBABABC	$P2_1cn$	40b	ABABACACBABC	*Pc*
19a	ABABCABCBCAC	$P2_1/c$	41	ABABACACBCAC	*Pc*
19b	ABABCABCBCAC	*P2/c*	42a	ABABACBABCBC	*Pc*
20a	ABABCACBACBC	*P2/c*	42b	ABABACBABCBC	*Pc*
20b	ABABCACBACBC	$P2_1/c$	43	ABABACBACABC	*Pc*
21a	ABABCACBCBAC	$P2_1cn$	44	ABABACBCACBC	*Pc*
21b	ABABCACBCBAC	$P2_1cn$	45a	ABABCABABCAC	*Pc*
22a	ABACBACBACBC	*P2/c*	45b	ABABCABABCAC	*Pc*
22b	ABACBACBACBC	$P2_1/c$	46a	ABABCABACABC	*Pc*
23	ABACBACBCABC	$P2_1cn$	46b	ABABCABACABC	*Pc*
24	ABACBCABACBC	*C2/c*	47a	ABABCABACBAC	*Pc*
25	ABABABABABAC	*Pc*	47b	ABABCABACBAC	*Pc*
26	ABABABABACAC	*Pc*	48a	ABABCABCABAC	*Pc*
27	ABABABABACBC	*Pc*	48b	ABABCABCABAC	*Pc*
28	ABABABACABAC	*Pc*	49a	ABABCABCACBC	*Pc*
29a	ABABABACACBC	*Pc*	49b	ABABCABCACBC	*Pc*
29b	ABABABACACBC	*Pc*	50	ABABCACBABAC	*Pc*
30	ABABABACBABC	*Pc*	51a	ABABCBABCBAC	*Pc*
31	ABABABACBCBC	*Pc*	51b	ABABCBABCBAC	*Pc*
32a	ABABABCABCAC	*Pc*	52	ABABCBACBCAC	*Pc*
32b	ABABABCABCAC	*Pc*	53	ABACABACBABC	*Pc*
33a	ABABABCABCBC	*Pc*	54	ABACABCBACBC	*Pc*

Notes: Pyroxenes 11–24 are in alphabetical order. Their structural parameters are in Table 5. Pyroxenes 25–54 are in alphabetical order and their structural parameters are in Table 6. Tables 5 and 6 are on deposit see note on page 5.

TABLE 7. Index table of pyroxenes

No.	Stacking sequence	SG*	Observed equivalent	Examples	SG*	Reference
1	ABAB	*C2/c*	H *I-C2/c* pyroxene	jadeite	*C2/c*	Clark et al. (1969)
				spodumene		Arlt and Angel (2000)
				$LiScSi_2O_6$		Arlt and Angel (2000)
				$NaScSi_2O_6$		Ohashi et al. (1994A)
				acmite		Redhammer et al. (2001)
				Kosmochlor		Origlieri et al. (submitted)
				$NaInSi_2O_6$		Ohashi et al. (1990)
				clinoferrosilite		Sueno et al. (1984)
2	ABAC	$P2_1cn$	protopyroxene	$Mg_{1.54}Li_{0.23}Sc_{0.23}Si_2O_6$	*Pbcn*	Yang et al. (1999)
			high-P protopyroxene	protoenstatite		Yang et al. (1999)
				$Mg_{1.54}Li_{0.23}Sc_{0.23}Si_2O_6$	$P2_1cn$	Yang and Ghose (1995)
3a	ABABCACABCBC	*P2/c*				
3b	ABABCACABCBC	$P2_1/c$	low clinopyroxene	spodumene	$P2_1/c$	Arlt and Angel (2000)
				$LiScSi_2O_6$		Arlt and Angel (2000)
				clinoenstatite		Pannhorst (1984)
				$MnSiO_3$		Tokonami et al. (1979)
				clinoferrosilite		Hugh-Jones et al. (1994)
4	ABCABCABCABC	*C2/c*	8-CN M2 clinopyroxene	hedenbergite	*C2/c*	Zhang et al. (1997)
				diopside		Levien and Prewitt (1981)
				johannsenite		Freed and Peacor (1967)
				$CaNiSi_2O_6$		Ghose et al. (1987)
				$CaCoSi_2O_6$		Ghose et al. (1987)
			H *P-C2/c* pyroxene	clinoferrosilite		Hugh-Jones et al. (1994)
5	ABABABAC	*Pc*				
6	ABABACBC	*Pc*				
7	ABABACAC	$P2_1ca$				
8a	ABABCABC	*P2/c*				
8b	ABABCABC	$P2_1/c$				
9a	ABABCBAC	*P2/c*				
9b	ABABCBAC	$P2_1/c$				
10	ABACBABC	$P2_1ca$	orthopyroxene	orthoferrosilite	*Pbca*	Sueno et al. (1976)
				orthoenstatite		Hugh-Jones and Angel (1994)
				$Co_2Si_2O_6$		Sasaki et al. (1982)

Note: Structural parameters for pyroxenes 1–4 are in Table 2, 5–6 are in Table 3, and 7–10 are in Table 4.
* SG = space group.

Alternate settings for pyroxenes

Some of the ideal pyroxenes have more than one possible setting. This section discusses the determination of our standard setting, what the alternatives are, and how to transform coordinates from the explicit cell setting to the standard setting, or to other possible settings. All of the transformation matrices presented below transform the coordinates of an atom as follows:

$$T_{D1\rightarrow D2}\begin{bmatrix}X\\Y\\Z\end{bmatrix}_{D1}=\begin{bmatrix}X'\\Y'\\Z'\end{bmatrix}_{D2}.$$

Our T matrices are equivalent to ***Q*** matrices in the *International Tables* (Arnold 1992).

We are especially interested in comparing the different cells for pyroxenes 1, 3b, and 4, as these can be thought of as H*T*-*C*2/*c* pyroxene (1), low clinopyroxene (3b), H*P*-*C*2/*c* pyroxene (4), and eight-coordinated M2 clinopyroxene (also 4). Both H*P*-*C*2/*c* pyroxene and eight-coordinated M2 clinopyroxene are based on cubic closest-packing of anions, but the eight-coordinated M2 clinopyroxenes are more distorted from ideal.

Figure 7 shows a partial symmetry diagram for pyroxene no. 1. The explicit cell has the same setting as an *I*2/*c* setting. The transformation to a *C*2/*c* setting can be derived from this diagram. The transformation matrix to change the coordinates of the atoms from *I*2/*c* to *C*2/*c* is:

$$T_{I2/c\rightarrow C2/c}=[\,[\mathbf{a}_{I2/c}]_{C2/c}\,|\,[\mathbf{b}_{I2/c}]_{C2/c}\,|\,[\mathbf{c}_{I2/c}]_{C2/c}\,]=\begin{bmatrix}1&0&0\\0&1&0\\1&0&1\end{bmatrix}.$$

From the diagram, $\cos\beta_{C2/c}=-c_{C2/c}/a_{C2/c}$, where $a_{C2/c}=(a_{I2/c}^2+c_{I2/c}^2)^{1/2}$. Changing β from 90° transforms the *a*-glide (not shown in Fig. 7) into an *n*-glide.

There is a more general method to find an unknown cell from a known alternate setting (Boisen and Gibbs 1985). The transformation matrix, T, is determined from a symmetry diagram. Then, from the circuit diagram,

$G_{D2}=T^{-t}G_{D1}T^{-1}$, where G is the metrical matrix (Boisen and Gibbs 1985). Given that the cell parameters of D1 are known, then G_{D2} can be constructed and the cell parameters for D2 are

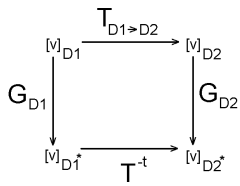

determined. This circuit diagram method is general and can be used to change the settings of any crystal.

Ideal pyroxene no. 4, the CCP *C*2/*c* pyroxene with β = 100.025°, has an *I*2/*c* setting with $\beta_{I2/c}=70.53°$. This pyroxene has an alternative *I*2/*c* setting with cell parameters identical to the standard cell of $P2_1/c$ pyroxene 3b (β = 109.47°), but the octahedra in this setting have –tilt because the direction of **c** is reversed. There is also a *C*2/*c* setting with –tilt, where β = $\cos^{-1}(-5/\sqrt{57})=131.46°$ ($\mathbf{a}_{131.46°}=\mathbf{a}_{100.025°}+2\mathbf{c}_{100.025°}$, $a=2\sqrt{19}r$).

Figure 8 is a partial symmetry diagram for pyroxene no. 3b. Axial ratios are not to scale so that the differences in β can be

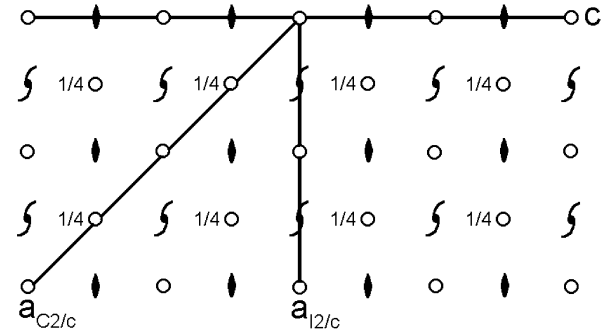

FIGURE 7. A partial symmetry diagram for hexagonal closest-packed clinopyroxene showing two different crystallographic settings.

exaggerated. The $P2_1/c$ axes labeled **a**1 and **c**1 correspond to the standard setting used for observed pyroxenes. In the ideal case, β = 109.47°. The transformation matrix from the explicit cell setting to this setting is

$$\begin{bmatrix}3&0&0\\0&1&0\\2&0&1\end{bmatrix}.$$

An alternative $P2_1/c$ setting with axes labeled **a**2 and **c**2 in Figure 8 has the same cell parameters as the standard cell for CCP pyroxene no. 4, with β = 100.025°. However, the octahedra have –tilt. Only one transformation matrix is necessary to go back and forth between the two $P2_1/c$ settings

$$\begin{bmatrix}1&0&0\\0&-1&0\\1&0&-1\end{bmatrix}.$$

Using the circuit diagram technique described above gives the formulas

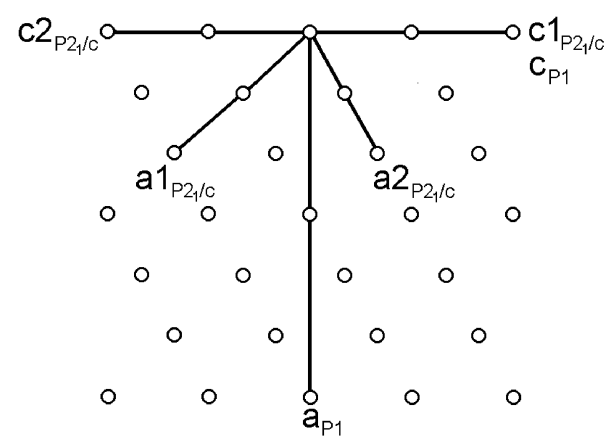

FIGURE 8. A partial symmetry diagram for ideal $P2_1/c$ closest-packed clinopyroxene showing three different crystallographic settings. The first $P2_1/c$ setting {**a**1, **b**1, **c**1} is the conventional choice of setting for observed pyroxenes. We used this diagram to go from our large explicit cell {**a**, **b**, **c**} to the conventional setting. All clinopyroxenes have an alternative setting {**a**2, **b**2, **c**2} wherein **a**2 = **a**1 + **c**1, **c**2 = –**c**1, and **b**2 = –**b**1. This setting reverses the octahedral tilt.

$a_2^2 = a_1^2 + c_1^2 + 2a_1c_1\cos\beta_1$

$\cos\beta_2 = (-c_1 - a_1\cos\beta_1)/(a_1^2 + c_1^2 + 2a_1c_1\cos\beta_1)^{1/2}$

This matrix and these formulas provide the information needed to transform between the *C*2/*c* and *I*2/*c* settings and between the two $P2_1/c$ settings.

Another setting for pyroxenes is obtained by reversing **b** and **c**. This also reverses the octahedral tilt, and the resulting β is the complement of the original β. Warren and Bragg's (1928) refinement of *C*2/*c* diopside, the first description of a pyroxene crystal structure, has β = 74.17°, and therefore an octahedral tilt opposite to today's convention.

Discussion

There are 81 ideal pyroxenes based on stacking sequences of length 12 or less, yet commonly observed pyroxene topologies are based on only five different ideal pyroxenes. Furthermore, a pyroxene with a fixed composition may assume more than one of these topologies, depending on pressure and temperature. Comparing the energetics of ideal pyroxenes may provide some insight to this behavior. It is straightforward to compare the energetics of ideal pyroxenes because bond energies are proportional to interatomic distances. For a given ideal anion radius, the first and second nearest neighbor anion-anion distances are equal in every ideal pyroxene. Furthermore, the anion-cation first and second nearest neighbor distances are equal, the M-M nearest neighbor distances are equal, and the T-T nearest neighbor distances are equal in every ideal pyroxene. The M2-T and M1-T distances between cations sharing coordination with O2 are the only nearest neighbor distances that change between structures, as illustrated in Figure 9. Thus, differences in the energetics of the various ideal pyroxene polymorphs depend only upon these M1-T and M2-T distances.

A feature of ideal pyroxenes is that they can be thought of as built from portions of HCP (no. 1) and CCP (no. 4) pyroxene, so that an understanding of the differences between these two can be readily extrapolated to an understanding of the important energetic features of any ideal pyroxene. While S-chains and O-chains have traditionally been associated with HCP and CCP, respectively, it is the relationship between a tetrahedral chain and the octahedral chain that shares O atoms with the tetrahedral chain's basal faces that is energetically important (Fig. 9). In the HCP portion of any ideal pyroxene, each tetrahedron shares an edge with an M2 octahedron (Sueno et al. 1976). Therefore, a shorter M2-T distance is found in an HCP portion than in a CCP portion: $R(\text{M2-T})_{\text{HCP}}/R(\text{M2-T})_{\text{CCP}} = \sqrt{17/33} = 0.72$. In contrast, the M1-T distance between cations sharing coordination with O2 is longer in an HCP portion of ideal pyroxenes than it is in a CCP portion: $R(\text{M1-T})_{\text{HCP}}/R(\text{M1-T})_{\text{CCP}} = \sqrt{41/33} = 1.11$. In CCP pyroxene, all M-T nearest neighbor distances are the same, $\sqrt{11/2}\,r$. In HCP pyroxene, *R*(M2-T) is significantly shorter than *R*(M1-T) for cations that share O2, $R(\text{M2-T})/R(\text{M1-T}) = \sqrt{17/33}/\sqrt{41/33} = 0.64$. Thus, the energetics of the M2-T interaction must have a significant impact on pyroxene topology.

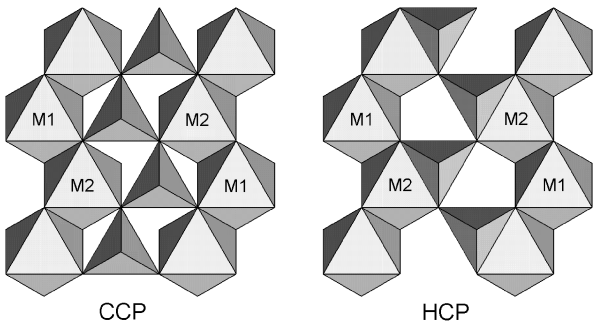

Figure 9. An illustration of CCP and HCP portions of ideal pyroxenes. All ideal pyroxenes are made up of combinations of these two configurations. An important difference between them is the short M2-T distance across the shared edge in the HCP portion.

Most room condition H*T*-*C*2/*c* pyroxenes have univalent M2 cations, while most pyroxenes with divalent M2 only assume H*T*-*C*2/*c* pyroxene topology at very high temperatures, if at all. The *C*2/*c* pyroxenes with divalent M2 at ambient conditions, such as diopside, usually assume the eight-coordinated M2 topology, a distortion of the ideal CCP pyroxene. The closer an O3-O3-O3 angle is to the ideal HCP value of 240°, the shorter the M2-T distance, so the force of this cation-cation repulsion is greater. H*T*-*C*2/*c* pyroxenes have the same bonding topology (Downs 2003) as HCP pyroxene, but their tetrahedral chains are approximately 180°, allowing a much longer M2-T distance than would occur in an ideal HCP pyroxene of equal volume. The *C*2/*c* pyroxenes with divalent M2 at ambient conditions, such as diopside, have O3-O3-O3 angles ~165°, and even longer M2-T distances.

The question remains: does M2-T repulsion control observed *C*2/*c* pyroxene topology or is some other factor dominant? Papike et al. (1973) correlated the O3-O3-O3 angle with average M-cation size, and suggested, "As the mean ionic radius decreases, the chains become straighter." Table 9 contains cation sizes and O3-O3-O3 angles for a number of ordered end-member silicate pyroxenes that are *C*2/*c* at room conditions. Figure 10 is the Papike et al. (1973) Figure 4, modified by including additional data. Cation sizes are from Shannon (1976). The solid line is the calculated relationship with $r_{\text{anion}} \equiv 1.36$ Å, the T and M1 sites are kept regular, and the M1 polyhedron is expanded by increasing the cation radius. The equation is

$$\cos(\angle\text{O3-O3-O3}) = -(3/4)(r_{\text{M1}}/r_{\text{anion}})^2 - (3/2)\,(r_{\text{M1}}/r_{\text{anion}}) + {}^1/_4.$$

The lack of agreement between the observed data points and the theoretical line suggests that cation size alone is not controlling topology. Some of the observed pyroxenes have both cation sizes significantly to the left of the line. We find that the O3-O3-O3 angle is more correlated with *R*(M2-T) than average cation size: $R^2 = 85.4\%$ vs. 44.8%.

We interpret this to mean that H*T*-*C*2/*c* pyroxene can form at ambient conditions only if the ratios of the sizes of the M cations to the T cation are such that a reasonably well-formed M1 can occur with an O3-O3-O3 angle that puts sufficient distance between M2 and T. If this requirement is met and a univalent cation is available for M2 in order to minimize repulsion, H*T*-*C*2/*c* pyroxene can form. The structure will distort so as to increase the M2-T distance as much as possible. If the M2 cation is divalent, the tetrahedral chains must rotate so far in the

TABLE 9. *M*-cation radii (Shannon 1976), O3-O3-O3 angles, and M-T distances for C2/c pyroxenes at ambient conditions

M2M1	r(M1) (Å)	r(M2) (Å)	<r(M)> (Å)	∠O3-O3-O3 (°)	M1-T	M2-T	Reference
LiAl	0.535	0.76	0.65	189.85	3.277	2.862	Arlt and Angel (2000)
LiFe	0.645	0.76	0.66	180.83	3.340	2.936	Redhammer et al. (2001)
LiGa	0.620	0.76	0.69	179.93	3.307	2.915	Sato et al. (1994)
LiV	0.640	0.76	0.70	178.07	3.361	2.915	Satto et al. (1987)
LiSc	0.745	0.76	0.75	175.63	3.425	2.961	Hawthorne and Grundy (1977)
NaAl	0.535	1.02	0.78	174.67	3.308	2.985	Clark et al. (1969)
NaMn	0.645	1.02	0.80	174.10	3.361	3.050	Ohashi et al. (1987)
NaFe	0.645	1.02	0.79	174.07	3.376	3.027	Redhammer et al. (2001)
NaTi	0.67	1.02	0.85	173.94	3.424	3.025	Ohashi et al. (1982)
NaSc	0.745	1.02	0.88	173.72	3.465	3.038	Ohashi et al. (1994A)
NaV	0.640	1.02	0.83	173.04	3.394	3.013	Ohashi et al. (1994B)
NaCr	0.615	1.02	0.82	172.79	3.379	2.995	Origlieri et al. (submitted)
NaGa	0.62	1.02	0.82	172.67	3.345	3.003	Ohashi et al. (1995)
NaIn	0.800	1.02	0.91	171.05	3.486	3.041	Ohashi et al. (1990)
CaMg	0.720	1.12	0.92	166.48	3.480	3.095	Levien and Prewitt (1981)
CaNi	0.69	1.12	0.91	165.19	3.474	3.097	Ghose et al. (1987)
CaCo	0.745	1.12	0.89	165.06	3.492	3.111	Ghose et al. (1987)
CaFe	0.78	1.12	0.87	164.37	3.511	3.126	Zhang (1997)
CaMn	0.83	1.12	0.90	163.78	3.561	3.126	Freed and Peacor (1967)
ZnZn	0.74	0.60	0.67	161.30	3.437	3.063	Morimoto et al. (1975)

O direction that the pyroxene adopts either the high-pressure topology (e.g., germanate pyroxenes) or the eight-coordinated M2 topology (e.g., diopside). In the special case of $ZnSiO_3$, the very small zinc cation is tucked so far away from the center of the M2 site and the silicon atom that it is only four-coordinated in both the H*T*-*C*2/*c* and H*P*-*C*2/*c* polymorphs (Morimoto et al. 1975; Arlt and Angel 2000; Downs 2003).

If *R*(M2-T) was the only crystal chemical consideration affecting pyroxene topology, then all pyroxenes would have fully rotated O-chains. A model pyroxene with regular M1, T, and fixed tetrahedral volume has maximum *R*(T-T) if the O3-O3-O3 angle is 180°. The topologies of the *C*2/*c* pyroxenes are compromises between T-T and M2-T repulsive forces. Univalent M2 minimizes M2-T repulsion and M2-O attraction, both forces that oppose extension of the tetrahedral chains toward the model E-chain O3-O3-O3 angle of 180°, so *C*2/*c* pyroxenes with univalent M2 can have O3-O3-O3 angles close to 180°. Divalent M2 increases the forces that oppose the straightening of the chains and *C*2/*c* pyroxenes with divalent M2 never have O3-O3-O3 angles much greater than 165° at room conditions.

The M2-T distance may also be important in the formation of orthopyroxene. When protoenstatite at high temperature is quenched rapidly, significant amounts of low clinoenstatite are produced (c.f. Smyth 1974). When quenched slowly, orthoenstatite predominates. In low clinopyroxene, there are alternating layers of nonequivalent tetrahedral chains. The TA-chains have short M2-T distances. In orthopyroxene, the TA-chains are O-chains, with longer M2-T distances. It may be that the short M2-T distance is driving the rotation of the TA chains from S-chains into O-chains during the transition, but, due to kinetics, significant time must be spent in the upper portion of the orthopyroxene temperature stability field for equilibration to occur. As an example, room condition M2-T distances for low clinoferrosilite (Hugh-Jones et al. 1994) and orthoferrosilite (Sueno et al. 1976) in the SiA chains are 2.73 Å and 2.88 Å, respectively, while the O3-O3-O3 angle are 193° and 169°.

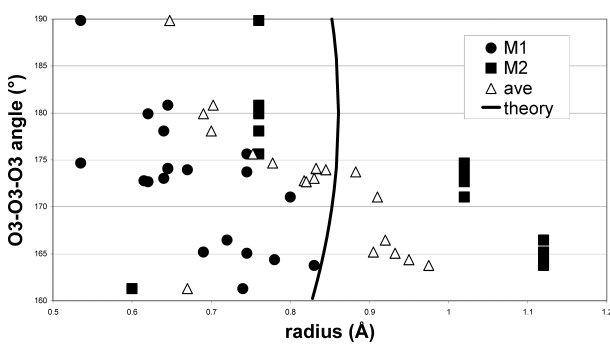

FIGURE 10. A plot of the O3-O3-O3 angles vs. M cation sizes for a variety of observed *C*2/*c* pyroxenes at ambient conditions, modified after Figure 4 of Papike et al. (1973). The solid line is the calculated relationship when $r_{anion} \equiv 1.36$ Å, the T and M1 sites are kept regular, and the M1 polyhedron is expanded by increasing the cation radius. There is an apparent correlation between average cation size and O3-O3-O3 angle, but the theoretical line suggests that cation size itself is not the actual reason for the trend.

Energy considerations

We created a simple electric potential to make a comparison of the energies of the ideal H*P*-*C*2/*c* pyroxene (no. 4), $P2_1ca$ orthopyroxene (no. 10), low clinopyroxene (no. 3b), $P2_1cn$ protopyroxene (no. 2), and H*T*-*C*2/*c* pyroxene (no. 1). We calculated a simple effective energy,

$$E_{eff} = \Sigma q_i q_j / R(ij),$$

for all atoms *i*,*j* in the structure where atoms *i* and *j* are bonded in observed equivalents, *i* is an O atom and *j* is a nearest neighbor O atom, or *i* is a cation and *j* is a neighboring cation.

This simple effective energy produces trends among ideal pyroxenes that parallel the sequence of phase transitions in observed equivalent structures (Fig. 11a). Electric potentials for ideal pyroxenes with divalent M2 increase in the following sequence: H*P*-*C*2/*c* pyroxene < $P2_1ca$ orthopyroxene < low clinopyroxene < $P2_1cn$ protopyroxene < H*T*-*C*2/*c* pyroxene. Electric potentials for ideal pyroxenes with univalent M2 fol-

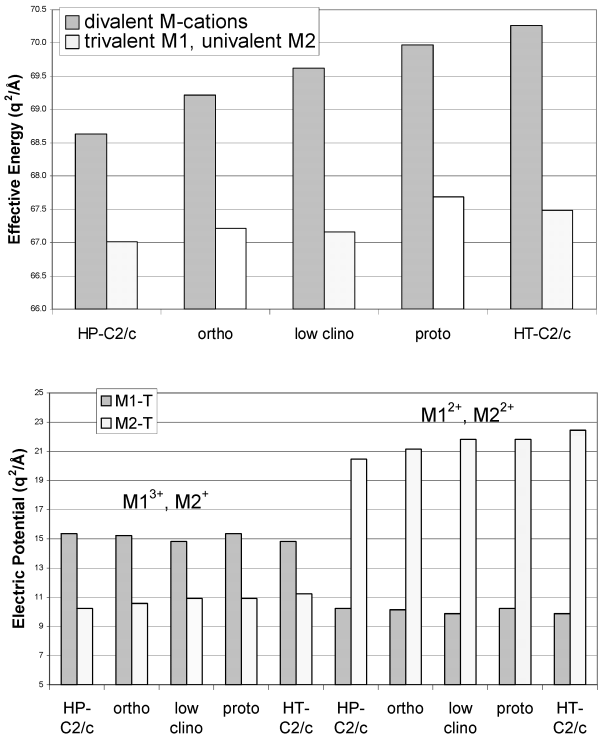

FIGURE 11. (**a**) Relative energies of ideal equivalents to observed pyroxenes calculated with a simple electric potential. Energetic trends parallel observed phase transitions. (**b**) Comparison of the electric potential energy for the M1-T and M2-T interactions as they vary between ideal pyroxene structures for $M1^{2+}$, $M2^{2+}$ and $M1^{3+}$, $M2^{+}$. Comparing Figures 11a and 11b reveals that the energy sequence of these ideal pyroxenes is determined entirely by a combination of M1-T and M2-T interactions.

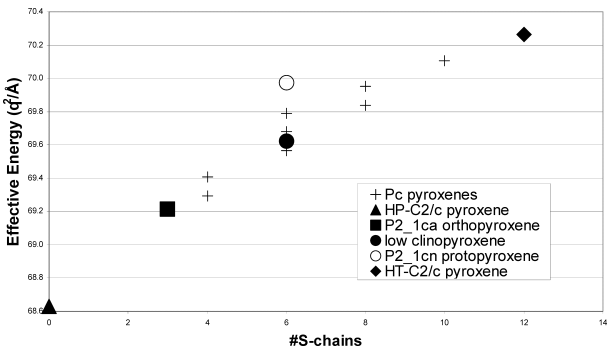

FIGURE 12. Relative energies calculated with a simple electric potential for the 45 12-monolayer ideal pyroxenes with space group *Pc* vs. the number of S-chains in the structure. These energies calculated for divalent M-cations. The 45 structures have eight different energies. Relative energies of ideal equivalents to observed pyroxenes added for comparison.

low a different sequence of increasing energy: H*P*-*C*2/*c* pyroxene < low clinopyroxene < $P2_1ca$ orthopyroxene < H*T*-*C*2/*c* pyroxene < $P2_1cn$ protopyroxene.

For a given arrangement of M-cation valences, the only parts of the effective energy that vary across different ideal pyroxene topologies are those related to the M1-T and M2-T interactions. Figure 11b illustrates how these potentials vary with structure for $M1^{2+}$, $M2^{2+}$ and $M1^{3+}$, $M2^{+}$. Comparing Figures 11a and 11b reveals that the energy sequence of these ideal pyroxenes is determined entirely by a combination of M1-T and M2-T interactions.

This simple potential does not explain why only five polymorphs commonly occur in nature. Figure 12 is a plot of effective energy for the 45 12-monolayer ideal pyroxenes with space group *Pc* vs. the number of S-chains per structure. These energies are calculated for divalent M-cations. The 45 structures have only eight different energies. Divalent M2 makes the M2-T interactions very important so that effective energy is loosely correlated with the number of S-chains in a structure. All of the chains in ideal H*T*-*C*2/*c* pyroxene are S-chains and this pyroxene has the highest effective energy. Yet, kanoite at 270 °C (Arlt and Armbruster 1997) is an example of an H*T*-*C*2/*c* pyroxene. What the effective energy does suggest is that observed equivalents of higher energy ideal pyroxenes should be more distorted than observed equivalents of lower energy ideal pyroxenes. It also suggests that both M1-T and M2-T interactions are important in determining pyroxene topologies and so are the M-cation valences.

ACKNOWLEDGMENTS

We thank Dr. M. Tribaudino and one anonymous reviewer for the their time and valuable suggestions. We also thank the National Science Foundation for funding our study, Compression Mechanisms of Upper Mantle Minerals, through grant No. EAR-9903104.

REFERENCES CITED

Angel, R.J., Chopelas, A., and Ross, N.L (1992) Stability of high-density clinoenstatite at upper-mantle pressures. Nature, 358, 322–324.

Arlt, T. and Angel, R.J. (2000) Displacive phase transitions in C-centered clinopyroxenes: spodumene, $LiScSi_2O_6$ and $ZnSi_2O_6$. Physics and Chemistry of Minerals, 27, 719–731.

Arlt, T. and Armbruster, T. (1997) The temperature-dependent $P2_1/c$-C2/c phase transition in the clinopyroxene kanoite $MnMg(Si_2O_6)$: a single-crystal X-ray and optical study. European Journal of Mineralogy, 9, 953–964.

Arnold, H. (1992) Transformations in crystallography. In T. Hahn, Ed., International Tables for Crystallography, Vol. A. Kluwer Academic Publishers, Boston.

Boisen, M.B. and Gibbs, G.V. (1985) Mathematical Crystallography. Reviews in Mineralogy, vol. 15, Mineralogical Society of America, Washington, D.C.

Boisen, M.B., Gibbs, G.V., and Bukowinski, M.S.T. (1994) Framework silica structures generated using simulated annealing with a potential-energy function—based on an $H_6Si_2O_7$ molecule. Physics and Chemistry of Minerals, 21, 269–284.

Cameron, M. and Papike, J.J. (1981) Structural and chemical variations in pyroxenes. American Mineralogist, 66, 1–50.

Clark, J.R., Appleman, D.E., and Papike, J.J. (1969) Crystal-chemical characterization of clinopyroxenes based on eight new structure refinements. Mineralogical Society of America Special Paper, 2, 31–50.

Deer, W.A., Howie, R.A., and Zussman, J. (1978) Rock-Forming Minerals, Volume 2A, Second Edition, Single Chain Silicates. Wiley, New York.

Downs, R.T. (2003) Topology of the pyroxenes as a function of temperature, pressure and composition determined from the procrystal electron density. American Mineralogist, 88, 556–566.

Freed, R.L. and Peacor, D.R. (1967) Refinement of the crystal structure of johannsenite. American Mineralogist, 52, 709–720.

Ghose, S., Wan, C., and Okamura, F.P. (1987) Crystal structures of $CaNiSi_2O_6$ and $CaCoSi_2O_6$ and some crystal-chemical relations in C2/c clinopyroxenes. American Mineralogist, 72, 375–381.

Hahn, T., Ed. (1995) International Tables for Crystallography, vol. A. Kluwer Academic Publishers, Boston.
Hattori, T., Nagai, T, Yamanaka, T., Werner, S., and Schulz, H. (2000) Single-crystal X-ray diffraction study of $FeGeO_3$ high-P clinopyroxene (C2/c) up to 8.2 GPa. American Mineralogist, 85, 1485–1491.
Hawthorne, F.C. and Grundy H.D. (1977) Refinement of the crystal structure of $LiScSi_2O_6$ and structural variations in alkali pyroxenes. Canadian Mineralogist, 15, 50–58.
Henry, N.F.M. and Lonsdale, K., Eds. (1965) International Tables for X-ray Crystallography, vol. I. Kynoch Press, Birmingham, England.
Hugh-Jones, D.A. and Angel, R.J. (1994) A compressional study of $MgSiO_3$ orthoenstatite up to 8.5 GPa. American Mineralogist, 79, 405–410.
Hugh-Jones, D.A., Woodland, A.B., and Angel, R.J. (1994) The structure of high-pressure C2/c ferrosilite and crystal chemistry of high-pressure C2/c pyroxenes. American Mineralogist, 79, 1032–1041.
Iijima, S. and Buseck, P.R. (1975) High resolution electron microscopy of enstatite I: twinning, polymorphism, and polytypism. American Mineralogist, 60, 758–770.
Law, A.D. and Whittaker, E.J.W. (1980) Rotated and extended model structures in amphiboles and pyroxenes. Mineralogical Magazine, 43, 565–574.
Levien, L. and Prewitt, C.T. (1981) High-pressure structural study of diopside. American Mineralogist, 66, 315–323.
Morimoto, N., Nakajima, Y., Syono, Y., Akimoto, S., and Matsui, Y. (1975) Crystal-structures of pyroxene-type $ZnSiO_3$ and $ZnMgSi_2O_3$. Acta Crystallographica, B31, 1041–1049.
Ohashi, H., Fujita, T., and Osawa, T. (1982) The crystal structure of the $NaTiSi_2O_6$ pyroxene. Journal of the Japanese Association of Mineralogists, Petrologists, and Economic Geologists, 77, 305–309.
Ohashi, H., Osawa T., and Tsukimura, K. (1987) Refinement of the structure of manganese sodium dimetasilicate. Acta Crystallographica, C43, 605–607.
Ohashi, H., Osawa T., and Sato, A. (1990) Structures of $Na(In,Sc)Si_2O_6$ clinopyroxenes formed at 6-Gpa pressure. Acta Crystallographica, B46, 742–747.
——— (1994a) $NaScSi_2O_6$. Acta Crystallographica, C50, 838–840.
——— (1994b) $NaVSi_2O_6$. Acta Crystallographica, C50, 1652–1655.
——— (1995) Low density form of $NaGaSi_2O_6$. Acta Crystallographica, C51, 2476–2477.
Origlieri, M., Downs, R.T., Thompson, R.M., Pommier, C.J.S., Denton, M.B., and Harlow, G. (2003) High-pressure crystal structure of Kosmochlor, $NaCrSi_2O_6$ and systematics of anisotropic compression of pyroxenes. American Mineralogist, in press.
Pannhorst, W. (1979) Structural relationships between pyroxenes. Neues Jahrbuch für Mineralogie Abhandlungen, 135, 1–17.
——— (1981) Comparison between topological classifications of pyroxenes. Neues Jahrbuch für Mineralogie Abhandlungen, 143, 1–14.
——— (1984) High temperature crystal structure refinements of low-clinoenstatite up to 700 °C. Neues Jahrbuch für Mineralogie Abhandlungen, 150, 270–279.
Papike, J.J., Prewitt, C.T., Sueno, S., and Cameron, M. (1973) Pyroxenes: comparisons of real and ideal structural topologies. Zeitschrift für Kristallographie, 138, 254–273.
Patterson, A.L. and Kasper, J.S. (1959) Close packing. In J.S. Kasper and K. Lonsdale, Eds., International Tables for X-ray Crystallography, Vol. II. Kynoch Press, Birmingham, England.
Peacor, D.R. (1968) The crystal structure of $CoGeO_3$. Zeitschrift für Kristallographie, 126, 299–306.
Redhammer, G.J., Roth, G., Paulus, W., André, G., Lottermoser, W., Amthauer, G., Treutmann, W., and Koppelhuber-Bitschnau, B. (2001) The crystal and magnetic structure of Li-aegerine $LiFe^{3+}Si_2O_6$: a temperature-dependent study. Physics and Chemistry of Minerals, 28, 337–346.
Sato, A., Osawa, T., and Ohashi, H. (1994) $LiGaSi_2O_6$. Acta Crystallographica, C50, 487–488.
Satto, C., Millet, P., and Galy, J. (1997) Lithium vanadium metasilicate, $LiVSi_2O_6$. Acta Crystallographica, C53, 1727–1728.
Shannon, R.D. (1976) Revised effective ionic radii and systematic studies of interatomic distances in halides and chalcogenides. Acta Crystallographica, A32, 751–767.
Smyth, J.R. (1974) Experimental study on the polymorphism of enstatite. American Mineralogist, 59, 345–352.
Sueno, S., Cameron, M., and Prewitt, C.T. (1976) Orthoferrosilite: high-temperature crystal chemistry. American Mineralogist, 61, 38–53.
Sueno, S., Kimata, M., and Prewitt, C.T. (1984) The crystal structure of high clinoferrosilite. American Mineralogist, 69, 264–269.
Thompson, J.B. (1970) Geometrical possibilities for amphibole structures: model biopyriboles. American Mineralogist, 55, 292–293.
Thompson, R.M. and Downs, R.T. (2001a) Quantifying distortion from ideal closest-packing in a crystal structure with analysis and application. Acta Crystallographica, B57, 119–127.
——— (2001b) Systematic generation of all nonequivalent closest-packed stacking sequences of length N using group theory. Acta Crystallographica, B57, 766–771.
Tokonami, M., Horiuchi, H., Nakano, A., Akimoto, S., and Morimoto, N. (1979) The crystal structure of the pyroxene-type $MnSiO_3$. Mineralogical Journal, 9, 424–426.
Tribaudino, M., Nestola, F., Camara, F., and Domenghetti, M.C. (2002) The high-temperature $P2_1/c \rightarrow C2/c$ phase transition in Fe-free pyroxene ($Ca_{0.15}Mg_{1.85}Si_2O_6$): structural and thermodynamic behavior. American Mineralogist, 87, 648–657.
Warren, B. and Bragg, W.L. (1928) XII. The structure of diopside, $CaMg(SiO_3)_2$. Zeitschrift für Kristallographie, 69, 168–193.
Yang, H. and Ghose, S. (1995) High temperature single crystal X-ray diffraction studies of the ortho-proto phase transition in enstatite, $Mg_2Si_2O_6$ at 1360 K. Physics and Chemistry of Minerals, 22, 300–310.
Yang, H. and Prewitt, C.T. (2000) Chain and layer silicates at high temperatures and pressures. In R.M. Hazen and R.T. Downs, Eds., High-Temperature and High-Pressure Crystal Chemistry, vol. 41, p. 211–255. Reviews in Mineralogy and Geochemistry, Mineralogical Society of America, Washington, D.C.
Yang, H., Finger, L.W., Conrad P.G., Prewitt, C.T., and Hazen, R.M. (1999) A new pyroxene structure at high pressure: single-crystal X-ray and Raman study of the Pbcn-$P2_1$cn phase transition in protopyroxene. American Mineralogist, 84, 245–256.
Zhang, L., Ahsbahs, H., Hafner, S., and Kutoglu, A. (1997) Single-crystal compression and crystal structure of clinopyroxene up to 10 GPa. American Mineralogist, 82, 245–258.

MANUSCRIPT RECEIVED AUGUST 11, 2002
MANUSCRIPT ACCEPTED NOVEMBER 22, 2002
MANUSCRIPT HANDLED BY ALESSANDRO GUALTIERI

APPENDIX

Subgroup–supergroup relations

Ideal pyroxene symmetries are subgroups of the symmetries of the stacking sequences they are constructed from. Listed below are subgroup-supergroup relationships (Hahn 1995) between ideal pyroxene symmetries and stacking sequence symmetries. The symbol (O) signifies that the stacking sequences for these pyroxenes have inversion centers on octahedral voids, (S) indicates inversion centers on anions, and (OS) sequences have both. The symbol (M) indicates that the $P2/c$ pyroxenes have cations at inversion centers (the $P2_1/c$ pyroxenes do not).

$Pc < P2/c < C2/c < P\bar{3}2/c1 < P\bar{3}m1$(S)	nos. 36,52,54
$Pc < Cc < Cm < P3m1$	nos. 29,32-35,37,38, 40,42,45-49,51(a,b)
$Pc < Cc < Cm < P3m1 < P\bar{6}m2$	nos. 5,6,25-28,30,31, 39,41,43,44,50,53
$Cc < Cm < P3m1 < P\bar{6}m2$	no. 16
$P2/c < C2/c < R\bar{3}2/c < R\bar{3}m$(O)(M)	no. 3a
$P2/c < C2/c < P\bar{3}2/c1 < P\bar{3}m1$(O) (M)	nos. (8,9,11,12)a, (14, 15)b, 17a, 19b, (20,22)a
$P2_1/c < C2/c < R\bar{3}2/c < R\bar{3}m$(O)	nos. 3b
$P2_1/c < C2/c < P\bar{3}2/c1 < P\bar{3}m1$(O)	nos. (8,9,11,12)b, (14, 15)a, 17b, 19a, (20,22)b
$C2/c < P\bar{3}2/c1 < P\bar{3}m1 < P6_3/mmc$(O)	nos. 1,24
$C2/c < R\bar{3}2/c < R\bar{3}m$(OS)	no. 4
$P2_1ca < Pbcn < Cmcm < P6_3/mmc$(S)	nos. 7,10
$P2_1cn < P2_1ca < Pbcn < Cmcm < P6_3/mmc$(S)	nos. 2,13,18, 23,
$P2_1cn < Cmc2_1 < P6_3mc$	nos. 21a,b

O3-O3-O3 angle calculations

Here we present some formulas for calculating the O3-O3-O3 angle in observed pyroxenes. We form two **O3-O3** vectors

and obtain the scalar product. The O3s are related by a *c*-glide perpendicular to **b**, so x_{O3} is constant and $x_{O3\text{-}O3} = 0$. The O3s are half a unit cell apart in the **c** direction, so $z_{O3\text{-}O3} = \pm 1/2$. Let Y = $y_{O3\text{-}O3}$ = twice the distance from the glide plane to O3 (i.e., distance along a line parallel to **b**). Then $\cos\theta = ([0\ Y\ 1/2]\ G\ [0\ Y - 1/2]^t) / ([0\ Y\ 1/2]\ G\ [0\ Y\ 1/2]^t)$. Unless otherwise noted, ∠O3-O3-O3 = θ.

*C*2/*c*: (if y_{O3} is close to 1, then $y = y_{O3} - 1$, otherwise $y = y_{O3}$)
$\cos\theta = (16y^2b^2 - c^2) / (16y^2b^2 + c^2)$
If $y < 0$, then ∠O3-O3-O3 = 360° − θ.

$P2_1/c$: O3A:$\cos\theta = [(1 - 4y)^2b^2 - c^2]/[(1 - 4y)^2b^2 + c^2]$
If $y > 1/4$, then ∠O3-O3-O3 = 360° − θ.
O3B: $\cos\theta = [(3 - 4y)^2b^2 - c^2] / [(3 - 4y)^2b^2 + c^2]$
If $y > 3/4$, then ∠O3-O3-O3 = 360° − θ.

Pbcn: Same as *C*2/*c* except if $y > 0$, then ∠O3-O3-O3 = 360° − θ.

Pbca: Same as $P2_1/c$ O3A.

Interatomic distance calculations

The square of the length of any vector, $[x\ y\ z]^t$, in a monoclinic basis, D = {**a**, **b**, **c**, 90, β, 90}, is

$a^2x^2 + 2ac\cos b xz + b^2y^2 + c^2z^2$.

We can form vectors between atoms of interest in terms of the asymmetric unit and use this formula to get their length. For cations sharing O2, M2-T = $[x_T - 1/2, y_T + y_{M2} - 1/2, z_T - 3/4]$ and M1-T = $[x_T - 1/2, y_T - y_{M1} + 1/2, z_T - 3/4]$. Therefore, $|M2\text{-}T|_{HCP} = \sqrt{17/6}$ and $|M1\text{-}T|_{HCP} = \sqrt{41/6}\,r$. For the two M1 cations sharing O1 with T, M1-T = $[x_T, y_T - y_{M1} + 1, z_T - 1/4]$ and $[x_T, y_T + y_{M1} - 1, z_T + 1/4]$.

O3-O3-O3 angle in terms of M1/T radius ratio

The O3-O3-O3 angle in terms of the M1/T radius ratio when T and M1 are regular can be obtained as follows:

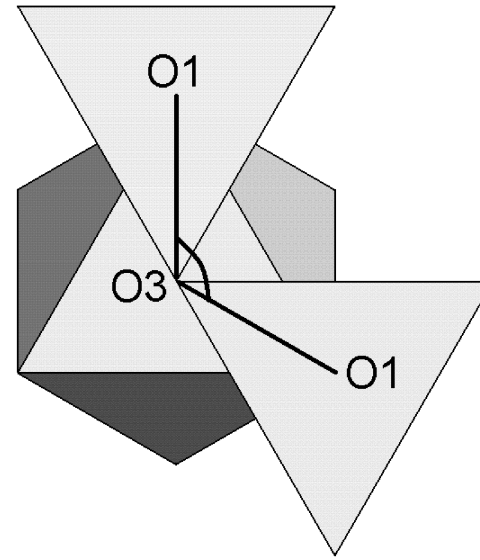

APPENDIX FIGURE 1. The O1-O3-O1 angle projected onto the **b-c** plane equals the O3-O3-O3 angle. If the tetrahedral edge length = 2*r*, then $|proj_{bc}(O1\text{-}O3)| = 2r/\sqrt{3}$ and $|O1\text{-}O1|^2 = (\text{octahedral edge})^2 = 2(2r/\sqrt{3})^2 - 2(2r/\sqrt{3})^2\cos(\angle O3\text{-}O3\text{-}O3)$.

axial M1 distance = $2r_{M1} + 2r_{anion}$.

Therefore, the length of the octahedral edge, *e*, is given by $e = \sqrt{2}\,(r_{M1} + r_{anion}) = |O1\text{-}O1|$.

The projection of the T-O3-T angle into the **b-c** plane is the same as the O3-O3-O3 angle (Appendix Fig. 1) and,

$proj_{bc}(|O1\text{-}O3|) = 2r/\sqrt{3}$.

Therefore,

$|O1\text{-}O1|^2 = e^2 = 2(2r/\sqrt{3})^2 - 2(2r/\sqrt{3})^2\cos(\angle O3\text{-}O3\text{-}O3)$.

Combining these results gives

$\cos(\angle O3\text{-}O3\text{-}O3) = -(3/4)(r_{M1}/r_{anion})^2 - (3/2)\,(r_{M1}/r_{anion}) + 1/4$.